Towards LoRa-Based LEO Satellite IoT: A Stochastic Geometry Perspective

Quantao Yu, Deepak Mishra, *Senior Member, IEEE*, Hua Wang, *Member, IEEE*, Dongxuan He, *Member, IEEE*, Jinhong Yuan, *Fellow, IEEE*, and Michail Matthaiou, *Fellow, IEEE*

***Abstract*—Recently, Long-Range (LoRa) based low Earth orbit (LEO) satellite Internet of Things (IoT) has garnered growing interest from both academia and industry, since it can guarantee pervasive connectivity in an energy-efficient and cost-effective manner. In this paper, we provide a novel spherical stochastic geometry (SG) based analytical framework for characterizing the uplink access probability of LoRa-based LEO satellite IoT system. Specifically, multiple classes of LoRa end-devices (EDs) are taken into consideration, where each class of LoRa EDs is modeled by an independent Poisson point process (PPP). Both the channel characteristics of the satellite-to-Earth communications and the unique features of the LoRa network are considered to derive closed-form analytical expressions for the uplink access probability of such a new paradigm. Moreover, the non-trivial impact of the spreading factor, the ED's density, the orbit altitude, and the satellite effective beamwidth on the system performance is thoroughly investigated. Extensive numerical simulations are conducted, which not only validate the accuracy of our theoretical analysis but also provide useful insights into the practical design and implementation of LoRa-based LEO satellite IoT system.**

***Index Terms*—Access probability, LoRa, performance analysis, satellite IoT, stochastic geometry.**

I. Introduction

THE recent years have witnessed the proliferation of low power wide area networks (LPWANs) in the Internet-of-Things (IoT), which aim to provide pervasive connectivity worldwide [2]. Among the state-of-the-art LPWAN technologies, Long-Range (LoRa) has attracted widespread attention from both academia and industry [3]. In general, LoRa can be categorized into two layers: a robust physical (PHY) layer using chirp spread spectrum (CSS) modulation (i.e., LoRa modulation) and a simple medium access control (MAC) layer underpinned by an ALOHA-based LoRaWAN protocol. Facilitated by its configurable radio parameters, such as carrier frequency (CF), bandwidth (BW), spreading factor (SF), and code rate (CR), LoRa promises a compelling trade-off between data rate and coverage, thus satisfying the various requirements of IoT applications [4].

Despite the immense success of LoRa technology, it is extremely challenging to provide ubiquitous coverage, especially in rural and remote areas (e.g., forests, deserts, and oceans), where terrestrial access is technically or economically impossible. In this context, exploiting LoRa-based low Earth orbit (LEO) satellite IoT has been regarded as a promising solution [5]. Recently, some experiments have verified the feasibility of LoRa-based radio links in space-to-Earth communications [6]–[8]. Moreover, supported by the LoRa ecosystem, several satellite operators have offered LoRa networks with satellite connectivity, delivering interoperability to address heterogeneous application domains, like asset tracking, energy development, and environmental monitoring [9]. While both technological and commercial traction have demonstrated its great potential for global connectivity, little attention has been paid to a holistic performance analysis of LoRa-based LEO satellite IoT system, which is of paramount significance to obtain deeper insights into such a new paradigm.

A. State-of-the-Art

Over the past few years, researchers have utilized stochastic geometry (SG), a powerful mathematical tool for analyzing and designing wireless networks, to investigate the performance of terrestrial LoRa networks. For example, the authors in [10] provided a SG-based analytical framework to investigate the uplink performance of a single gateway LoRa network and showed that the coverage probability drops exponentially as the number of end-devices (EDs) grows due to the same SF (co-SF) interference. Based on this model, the authors in [11] investigated the uplink performance improvements of LoRa networks by exploiting time diversity through message replication and spatial diversity through multiple antennas. Moreover, both the co-SF interference and different SF (inter-SF) interference were taken into account in [12] to investigate

This work was supported in part by the National Key Research and Development Program of China under Grant 2024YFE0200404; in part by the National Key Research and Development Program of China under Grant 2020YFB1807900; in part by the China Scholarship Council (CSC); and in part by the U.K. Engineering and Physical Sciences Research Council (EPSRC) (grant No. EP/X04047X/1). This work was partially funded by the Australian Research Council (ARC) Discovery Early Career Researcher Award (DECRA) - DE230101391. The work of M. Matthaiou has received funding from the European Research Council (ERC) under the European Union's Horizon 2020 research and innovation programme (grant agreement No. 101001331). *(Corresponding authors: Hua Wang; Dongxuan He.)*

Quantao Yu, Hua Wang, and Dongxuan He are with the School of Information and Electronics, Beijing Institute of Technology, Beijing 100081, China, (e-mails: 3120215432@bit.edu.cn; wanghua@bit.edu.cn; dongxuan_he@bit.edu.cn).

Deepak Mishra and Jinhong Yuan are with the School of Electrical Engineering and Telecommunications, University of New South Wales Sydney, NSW 2052, Australia, (e-mails: d.mishra@unsw.edu.au; j.yuan@unsw.edu.au).

Michail Matthaiou is with the Centre for Wireless Innovation (CWI), Queen's University Belfast, BT3 9DT Belfast, U.K., (e-mail: m.matthaiou@qub.ac.uk).

A preliminary conference version of this work has been accepted for presentation at the 2025 IEEE ICC conference [1].

TABLE I
COMPARISON OF RELATED WORKS

Reference	Main work	Small-scale fading
[10]	Investigated the coverage probability of a terrestrial LoRa network with co-SF interference under the PPP EDs' model	Rayleigh fading
[11]	Investigated the coverage probability of a terrestrial LoRa network with co-SF interference, time and spatial diversity under the PPP EDs' model	Rayleigh fading
[12]	Investigated the coverage probability of a terrestrial LoRa network with co-SF and inter-SF interference under the PPP EDs' model	Rayleigh fading
[13]	Investigated the coverage probability of a terrestrial LoRa network with co-SF interference and SIC under the PPP EDs' model	Rayleigh fading
[14]	Investigated the coverage probability of a terrestrial LoRa network with intra- and inter-network interference under the PCP EDs' model	Rayleigh fading
[15]	Investigated the coverage probability and ASE of a terrestrial LoRa network with co-SF interference under the PPP EDs' model	Nakagami-m fading
[18]	Investigated the coverage probability of an IoT-over-satellite network under the PPP constellation model	-
[19]	Investigated the outage probability of a star-of-star LEO satellite IoT network under the BPP constellation model	SR fading
[20]	Investigated the uplink access probability of a LoRa-based LEO satellite IoT network based on a planar SG framework	Rician fading
[21]	Investigated the coverage probability of an IoT-over-satellite network under the BPP constellation and PCP EDs' model	Rayleigh fading SR fading
Our work	Investigated the uplink access probability of LoRa-based LEO satellite IoT systems based on a novel spherical SG framework	SR fading

the scalability of LoRa networks. It was also shown that co-SF interference plays a dominant role in interference-limited scenarios since different SFs are quasi-orthogonal. Furthermore, the system model proposed in [13] combined power-domain non-orthogonal multiple access (NOMA) and successive interference cancellation (SIC) which could significantly increase the LoRa networks' scalability.

Notably, the spatial distribution of EDs was described through Poisson point process (PPP) in [10]–[13] which can accurately model the networks when the LoRa EDs are uniformly distributed in a considered area. However, when the LoRa EDs are clustered, the PPP is no longer a suitable choice to model the EDs' spatial distribution. To address this issue, the authors in [14] proposed to use Poisson cluster process (PCP) to model LoRa networks, where the LoRa gateways form the parent process and the active LoRa EDs in each cluster form the children process. Moreover, to obtain a more tractable framework of the coverage probability and area spectral efficiency, the authors in [15] took into consideration the Nakagami-m fading rather than the Rayleigh fading adopted in most previous works. Based on the derived theoretical expressions for the coverage probability and area spectral efficiency, the trends of both metrics were unveiled with respect to some key system parameters, such as the transmit power, the ED's density, and the SF.

In addition, analytical modeling and performance analysis based on SG have also been recently leveraged in satellite networks, which paves the way to study the generic performance of LEO satellite networks without relying on specialized software platforms [16], [17]. With regard to the satellite IoT networks, the authors in [18] investigated the coverage probability of IoT-over-satellite network with intra-network interference under the PPP constellation model. Besides, the authors in [19] proposed a star-of-star topology to effectively leverage the spatial diversity of multiple satellites, modeled by Binomial point process (BPP), to achieve the desired outage probability performance in LEO satellite IoT networks. Additionally, the authors in [20] investigated the uplink access probability of LoRa-based LEO satellite IoT network based on a planar SG framework under the PPP EDs' model, while the authors in [21] focused on the coverage probability of IoT-over-satellite network with intra-network interference under the BPP constellation and PCP EDs' model.

B. Motivation and Contributions

Herein, all the above mentioned works are summarized in Table I for a detailed comparison. Although these works have

laid a solid foundation for the performance analysis of either terrestrial LoRa networks or LEO satellite IoT networks, few of them have focused on SG-based network modeling and performance analysis of LoRa-based LEO satellite IoT systems. The most relevant existing works on this topic are [20] and [21]. However, the system model presented in [20] inherently followed the terrestrial LoRa network paradigm based on a planar SG framework, where the LoRa EDs were assumed to be distributed within a circle area and only the strongest interfering ED is considered, which leads to an inaccurate interference characterization and thereby significantly limits its findings within the LEO satellite IoT space. Moreover, the system model proposed in [21] did not take into account the unique features of LoRa networks, like CSS modulation, SF allocation, and radio duty cycle, which however play a dominant role in determining the overall performance of LoRa-based LEO satellite IoT systems. Therefore, to accurately characterize the uplink performance of LoRa-based LEO satellite IoT system, we present a novel spherical SG-based analytical framework for the uplink access probability in this paper, where both the channel characteristics of the satellite-to-Earth communications and the unique features of the LoRa network are incorporated into our proposed system model, thus enabling a rigorous scalability analysis of such a new paradigm while facilitating its practical design and implementation. The main contributions of this paper are summarized as follows:

1) A novel spherical SG-based analytical framework for characterizing the uplink access probability of LoRa-based LEO satellite IoT is developed. Specifically, multiple classes of LoRa EDs are taken into consideration, where each class of EDs is modeled by an independent PPP. Both the channel characteristics of the satellite-to-Earth communications and the unique features of the LoRa network are considered in our system model. The impact of shadowed Rician (SR) fading, CSS modulation, SF allocation, and duty cycle-limited random access is investigated, thus enabling an accurate uplink access probability analysis of such a new paradigm.
2) To give a comprehensive performance analysis, we derive closed-form analytical expressions for the uplink access probability in both interference-free and interference-limited scenarios. We start with the interference-free scenario to obtain insights into the ideal access probability which serves as an upper bound for the practical system performance. The Laplace transform (LT) of the aggregated interference is derived to obtain an analytical expression of the access probability in the interference-limited scenario. Moreover, to reduce the computational complexity, an approximate closed-form expression of the access probability is derived where the aggregated interference converges to the mean value.
3) The non-trivial impact of some key system parameters, including the SF, the ED's density, the orbit altitude, and the satellite effective beamwidth, on the system performance is thoroughly investigated. Extensive numerical simulations are conducted to verify the accuracy of our theoretical analysis, which can provide insightful guidelines for the practical design and implementation of LoRa-based LEO satellite IoT system. Moreover, we clarify some open issues and future research directions in this field, which can further shed light into the performance improvements of the underlying system.

TABLE II
LIST OF IMPORTANT NOTATIONS

Notation	Meaning
R	Radius of Earth
H	Orbit altitude
$\mathcal{R}$	Satellite footprint
ψ	Satellite effective beamwidth
φ, φ_m	Contact angle, maximum contact angle
d	Contact distance
$\mathcal{K}$	Total number of ED's classes
Φ	PPP of the LoRa EDs
λ	Intensity of Φ
Φ_k, Φ_k^A	PPP of EDs and active EDs of class k
λ_k	Intensity of Φ_k
ρ_k	SF allocation proportion of class k
p_k	Active probability of class k
$\bar{N}_k$	Average number of EDs of class k
P_t	Effective isotropic radiated power of EDs
T_k	Time on Air of class k
T_p	Average packet inter-arrival time
f_c	Carrier frequency
$L(\cdot)$	Free space path-loss
m, b_0, Ω	SR fading parameters
α, β	Gamma distribution parameters
$\varphi_{o,k}$, $\varphi_{i,k}$	Earth-centered zenith angle of typical and interfering EDs of class k
r_k	Received signal of class k
$h_{o,k}$, $h_{i,k}$	Small-scale fading from the typical and interfering EDs of class k
$s_{o,k}$, $s_{i,k}$	Transmitted signal from the typical and interfering EDs of class k
w	Additive white Gaussian noise
G	Satellite antenna gain
σ^2	Noise power
N_F	Receiver's noise figure
B_W	Channel bandwidth
P_s	Access probability
P_{SNR}	Connection probability
P_{SIR}	Capture probability
γ_k	SNR threshold of class k
γ_I	SIR threshold for successful reception
κ	Interference mitigation factor
I_k	Aggregated interference of class k
$\bar{I}_k$	Average aggregated interference of class k
P_{SIR}°	Approximate capture probability
P_s°	Approximate access probability

C. Paper Organization and Notations

The rest of the paper is organized as follows: Section II presents the system model of LoRa-based LEO satellite IoT, followed by the uplink performance analysis in Section III. Simulation results are provided in Section IV to validate our theoretical analysis where we also point out some open issues along with the future research directions. Finally, we conclude the whole paper in Section V.

Notation: Throughout this paper, we denote $F_X(x)$ and $f_X(x)$ as the cumulative distribution function (CDF) and the probability density function (PDF) of a random variable X; $\max\{\cdot\}$, $\lceil\cdot\rceil$, $\binom{\cdot}{\cdot}$, $\exp(\cdot)$, and $\ln(\cdot)$ are the maximum, ceiling, binomial coefficient, natural exponential, and natural logarithm operations; $\mu!$ is the factorial of μ; $\mathbb{E}[\cdot]$ and $\Pr\{\cdot\}$ denote the mathematical expectation and probability measure, respectively. The LT of a random variable X is defined as $\mathcal{L}_X(\nu) = \mathbb{E}\left[e^{-\nu X}\right]$ with $\nu \in \mathbb{C}$. Besides, $|\mathcal{R}|$ represents the coverage area of satellite footprint $\mathcal{R} \in \mathbb{R}^d$. For the reader's convenience, the main notations used in this paper are summarized in Table II.

II. System Model

In this section, we present the analytical framework of our considered LoRa-based LEO satellite IoT system, including the network model, channel model, and signal model.

A. Network Model

In this paper, we consider a single LEO satellite that directly communicates with the terrestrial LoRa EDs within its coverage region.

1) Geometric model: Without loss of generality, we denote H as the orbit altitude of the LEO satellite while the terrestrial LoRa EDs are randomly and uniformly distributed within its coverage region, i.e., satellite footprint $\mathcal{R}$, which is determined by the effective beamwidth of serving satellite. Accordingly, we denote the satellite effective beamwidth as ψ, which corresponds to the maximum satellite-centric angle as depicted in Fig. 1. Moreover, to simplify the mathematical representation, we use the contact angle φ to denote the relative location between a LoRa ED and serving satellite, i.e., the Earth-centered zenith angle. According to the basic sine theorem, the maximum contact angle φ_m can be derived as [22]

$$\varphi_m = \begin{cases} \sin^{-1}\left(\frac{R+H}{R}\sin\left(\frac{\psi}{2}\right)\right) - \frac{\psi}{2}, & \text{if } \psi < \psi_0 \\ \cos^{-1}\left(\frac{R}{R+H}\right), & \text{if } \psi \geq \psi_0, \end{cases} \tag{1}$$

where R is the radius of Earth and $\psi_0 = 2\sin^{-1}\left(\frac{R}{R+H}\right)$ denotes the effective beamwidth corresponding to just covering the horizon.

As a result, the coverage area of the satellite footprint can be obtained as [22]

$$|\mathcal{R}| = 2\pi R^2 (1 - \cos\varphi_m). \tag{2}$$

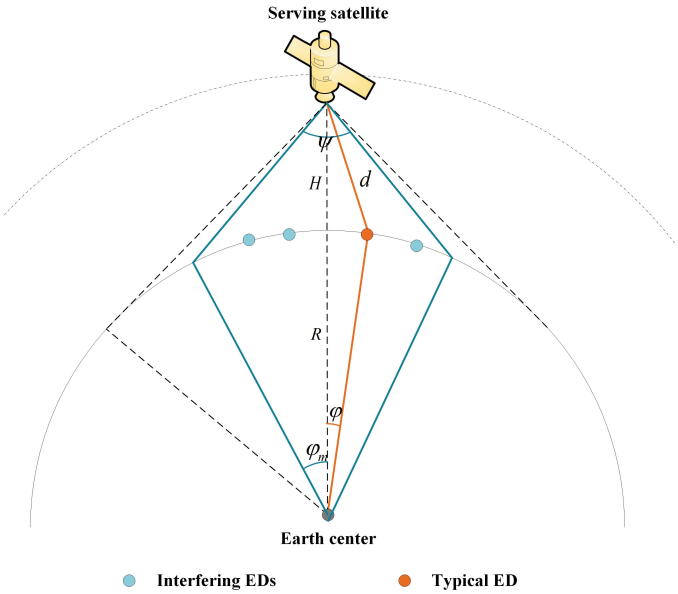

Fig. 1. An illustration of the geometric model of LoRa-based LEO satellite IoT including the satellite footprint, effective beamwidth ψ, contact angle φ, and contact distance d.

Given the contact angle φ, the distance between the ED and serving satellite, i.e., contact distance, can be obtained using the basic cosine theorem as [22]

$$d(\varphi) = \sqrt{(R+H)^2 + R^2 - 2R(R+H)\cos\varphi}. \tag{3}$$

2) EDs' model: In the context of LEO satellite IoT scenarios, the EDs are often widely deployed in open areas, like environmental monitoring and smart agriculture [5], [7], and thus a uniform distribution of the deployed EDs is a reasonable assumption and appropriate modeling technique for SG-based analysis [18]–[20]. Therefore, the LoRa EDs within our considered system are assumed to be uniformly distributed within the satellite footprint, i.e., the spherical area $\mathcal{R}$, whereas the distribution of the LoRa EDs is modeled by a PPP Φ with intensity λ (i.e., ED's density).

Let us consider that there are $\mathcal{K}$ classes of LoRa EDs deployed within the satellite footprint. Each class of EDs is assigned with one SF and modeled by an independent PPP Φ_k where $k \in \{7, ..., 12\}$. Typically, a set of SFs ranging from 7 to 12 are adopted in LoRa networks. Hence, we have $\mathcal{K} = 6$. Two SF allocation schemes are considered, namely, random allocation and fair-collision allocation, for the uplink access of our considered LoRa-based LEO satellite IoT system. In particular,

- Under a random allocation scheme, each ED is randomly assigned a SF and the proportion that an ED is assigned the SF k is $\rho_k = \frac{1}{6}, \forall k$.
- Under a fair-collision allocation scheme, the proportion that an ED is assigned the SF k is given by [15]

$$\rho_k = \frac{k/2^k}{\sum_{i=7}^{12} i/2^i}, \tag{4}$$

which guarantees a fair collision probability among all classes of EDs.

Therefore, the density of EDs of class k is given by $\lambda_k = \rho_k \lambda$. As a result, the number of EDs of class k is a Poisson random variable and its mean value can be computed as

$$\bar{N}_k = \lambda_k |\mathcal{R}| = 2\pi \rho_k \lambda R^2 \left(1 - \cos \varphi_m\right). \tag{5}$$

All classes of EDs are equipped with an omnidirectional antenna with the same effective isotropic radiated power (EIRP) denoted as P_t. Moreover, we denote Φ_k^A as the set of active EDs of class k, which also follows a PPP with intensity $p_k \lambda_k$, where $p_k = \frac{T_k}{T_p}$ is the active probability of class k with T_k and T_p representing the Time on Air (ToA) of class k and the average packet inter-arrival time, respectively.

Specifically, the configurations of BW, SF, and CR impact the ToA of class k, which can be formulated as [15]

$$T_k = \left(N_{pre} + 4.25 + N_{pay}\right) \frac{2^k}{B_W}, \tag{6}$$

where B_W is the configured BW, N_{pre} and N_{pay} denote the number of CSS symbols in the preamble and the PHY payload, respectively, and [15]

$$N_{pay} = \max\left\{ \left\lceil \frac{8P_L - 4k + 28 + 16C - 20H_E}{4k} \right\rceil (C_R + 4), 0 \right\} + 8, \tag{7}$$

where P_L denotes the PHY payload length in bytes, $C_R \in \{1, 2, 3, 4\}$ denotes the CR, C indicates the presence (i.e., $C = 1$) or absence (i.e., $C = 0$) of cyclic redundancy check (CRC), $H_E = 0$ indicates that the PHY layer header is enabled, while $H_E = 1$ indicates that the PHY layer header is not enabled.[1]

B. Channel Model

In this paper, both large-scale fading and small-scale fading are taken into consideration.

1) Large-scale fading: For the sake of simplicity, we adopt the free space path-loss model to characterize the large-scale fading[2], which is suitable for the Internet of remote things where the EDs are typically distributed in open remote areas (e.g., forests, deserts, and oceans) [23]. Specifically, given the transmission distance $d(\varphi)$ and the CF f_c, the free space path-loss is given as [23]

$$L\left(d\left(\varphi\right)\right) = \left(\frac{c}{4\pi f_c d\left(\varphi\right)}\right)^2, \tag{8}$$

where c refers to the speed of light.

2) Small-scale fading: Let us denote $h_{o,k}$ and $h_{i,k}$ as the small-scale fading from the typical and interfering devices of class k to the serving satellite, respectively, which follows an independent and identically distributed (i.i.d.) SR fading with Nakagami fading coefficient m, where the half average power of scattered component is b_0 and the average power of line-of-sight component is Ω. As such, the CDF and PDF of the SR channel gain $|h|^2$ are given by [24]

$$F_{|h|^2}\left(x\right) = \left(\frac{2b_0 m}{2b_0 m + \Omega}\right)^m \sum_{z=0}^{\infty} \frac{\left(m\right)_z}{z!\Gamma\left(z+1\right)} \left(\frac{\Omega}{2b_0 m + \Omega}\right)^z \times \gamma\left(z+1, \frac{1}{2b_0} x\right), \tag{9}$$

$$f_{|h|^2}\left(x\right) = \left(\frac{2b_0 m}{2b_0 m + \Omega}\right)^m \frac{1}{2b_0} \exp\left(-\frac{x}{2b_0}\right) \times {}_1F_1\left(m, 1, \frac{\Omega x}{2b_0\left(2b_0 m + \Omega\right)}\right), \tag{10}$$

respectively, where $\Gamma(\cdot)$ denotes the Gamma function, $\gamma(\cdot,\cdot)$ is the lower incomplete gamma function, $(\cdot)_z$ is the Pochhammer symbol, while ${}_1F_1(\cdot,\cdot,\cdot)$ is the confluent hypergeometric function [24]. Note that (9) and (10) are too complex to manipulate and, thus, we approximate the SR channel gain $|h|^2$ by a Gamma random variable with its CDF and PDF as [21]

$$F_{|h|^2}\left(x\right) \approx \frac{1}{\Gamma\left(\alpha\right)} \gamma\left(\alpha, \frac{x}{\beta}\right), \; x \geq 0, \tag{11}$$

$$f_{|h|^2}\left(x\right) \approx \frac{1}{\beta^\alpha \Gamma\left(\alpha\right)} x^{\alpha-1} \exp\left(-\frac{x}{\beta}\right), \; x \geq 0, \tag{12}$$

where $\alpha \triangleq \frac{m(2b_0+\Omega)^2}{4mb_0^2+4mb_0\Omega+\Omega^2}$ and $\beta \triangleq \frac{4mb_0^2+4mb_0\Omega+\Omega^2}{m(2b_0+\Omega)}$ denote the shape and scale parameters, respectively. The accuracy of this approximation will be shown in Section IV-A.

C. Signal Model

Let us denote $s_{o,k}$ and $s_{i,k}$ as the unit power transmitted signal from the typical and interfering devices of class k, respectively, i.e., $\mathbb{E}\left[|s_{o,k}|^2\right] = \mathbb{E}\left[|s_{i,k}|^2\right] = 1$. Similar to the methods employed in [18], we denote $\kappa \in [0,1]$ as the interference mitigation factor, which captures the impact of random access on the received signal and underpins the flexibility of performance analysis. In particular, $\kappa = 0$ represents an ideal interference-free system, while $\kappa = 1$ represents the worst-case scenario corresponding to ALOHA-based system. For our considered LoRa-based LEO satellite IoT system, inter-ED interference consists of co-SF interference and inter-SF interference. Given the waveform properties of CSS modulation, different SFs are quasi-orthogonal and thus the impact of inter-SF interference can be considered negligible [10], [15]. Accordingly, the received signal of class k can be expressed as

$$r_k = \underbrace{\sqrt{P_t G L\left(d\left(\varphi_{o,k}\right)\right)} h_{o,k} s_{o,k}}_{\text{desired signal}} + \underbrace{w}_{\text{noise}} + \underbrace{\kappa \sum_{i \in \Phi_k^A} \sqrt{P_t G L\left(d\left(\varphi_{i,k}\right)\right)} h_{i,k} s_{i,k}}_{\text{interfering signal}}, \tag{13}$$

where G represents the satellite antenna gain, w represents the complex circularly symmetric additive white Gaussian noise (AWGN) with zero mean and variance $\sigma^2 = -174 + N_F +$

[1] In this paper, we assume that $N_{pre} = 8$, $C = 1$, $H_E = 0$, and $C_R = 1$ [15].

[2] It is worth noting that some of the literature also takes into consideration the additional path-loss caused by atmospheric absorption and natural/artificial obstacles [22]. However, the corresponding channel model is more suitable for urban environments. Meanwhile, it can be easily integrated into our channel model by adding the excess path-loss factor into the large-scale fading.

$10\log_{10} B_W$, with N_F representing the receiver's noise figure. We point out that the Doppler effect is not taken into account in the signal model for simplicity since both laboratory and flight testings have verified the strong immunity of LoRa-based LEO satellite communications to it [8].

III. Uplink Performance Analysis

To evaluate the uplink performance of LoRa-based LEO satellite IoT system, we define the access probability as the performance metric which measures the probability of successful transmission, i.e., the desired signal can be successfully demodulated. In particular, the access probability P_s is defined as [7], [10]

$$P_s = P_{SNR} P_{SIR}, \tag{14}$$

where P_{SNR} and P_{SIR} denote the connection probability and the capture probability, respectively. Specifically, the connection probability P_{SNR}, represents the probability of signal-to-noise ratio (SNR) of the desired signal received by the LEO satellite exceeding the SF-specific demodulation threshold. Moreover, the capture probability P_{SIR}, represents the probability of signal-to-interference ratio (SIR) of the desired signal received by the LEO satellite exceeding a predefined interference rejection threshold. Therefore, the successful transmission occurs only if both the SNR and SIR of the received desired signal exceed their corresponding thresholds. In the following, we will provide a detailed analysis of both the connection probability and the capture probability.

A. Connection Probability

We start with the interference-free scenario, i.e., $\kappa = 0$, to obtain insights into the ideal access probability, i.e., connection probability, which serves as an upper bound for the uplink access probability of practical systems. Specifically, the connection probability, P_{SNR}, can be derived according to the signal model (13) as

$$\begin{aligned} P_{SNR} &= \Pr\left\{ \frac{\mathbb{E}\left[\left| \sqrt{P_t G L\left(d\left(\varphi_{o,k}\right)\right)} h_{o,k} s_{o,k} \right|^2 \right]}{\mathbb{E}\left[|w|^2\right]} \geq \gamma_k \right\} \\ &= \Pr\left\{ \frac{P_t G L\left(d\left(\varphi_{o,k}\right)\right) |h_{o,k}|^2}{\sigma^2} \geq \gamma_k \right\} \\ &= \Pr\left\{ |h_{o,k}|^2 \geq \frac{\sigma^2 \gamma_k}{P_t G L\left(d\left(\varphi_{o,k}\right)\right)} \right\} \\ &= 1 - F_{|h_{o,k}|^2}\left(\frac{\sigma^2 \gamma_k}{P_t G L\left(d\left(\varphi_{o,k}\right)\right)} \right) \\ &\overset{(a)}{\approx} 1 - \frac{1}{\Gamma(\alpha)} \gamma\left(\alpha, \frac{\sigma^2 \gamma_k}{\beta P_t G L\left(d\left(\varphi_{o,k}\right)\right)} \right), \end{aligned} \tag{15}$$

where γ_k is the SF-specific SNR threshold while step (a) follows directly from the substitution of the CDF described in (11).

Remark 1: The connection probability P_{SNR} is related to the link budget and is independent of the ED's density. However, since its MAC layer protocol is essentially an ALOHA-based variant, LoRa-based LEO satellite IoT systems will inevitably become interference-limited in the scope of dense network deployments, thus leading to an interference-dependent performance analysis.

B. Capture Probability

In general, the desired transmitted signal of class k in the presence of interference can be demodulated only if the capture effect (CE) occurs, i.e., the SIR of the desired signal is above the corresponding threshold. As such, the capture probability, P_{SIR}, can be formulated according to the signal model (13) as

$$P_{SIR} = \Pr\left\{ \frac{P_t G L\left(d\left(\varphi_{o,k}\right)\right) |h_{o,k}|^2}{\kappa \sum_{i \in \Phi_k^A \setminus o} P_t G L\left(d\left(\varphi_{i,k}\right)\right) |h_{i,k}|^2} \geq \gamma_I \right\}. \tag{16}$$

For an accurate performance analysis, we need to investigate the statistical distribution of the accumulative co-SF interference for class k in (16). Herein, we denote I_k as the accumulative co-SF interference for class k, which can be obtained according to (16) as

$$I_k = \kappa \sum_{i \in \Phi_k^A \setminus o} P_t G L\left(d\left(\varphi_{i,k}\right)\right) |h_{i,k}|^2. \tag{17}$$

Since the statistical distribution of I_k cannot be obtained directly from (17), we rewrite the capture probability in (16) as

$$\begin{aligned} P_{SIR} &= \Pr\left\{ \frac{P_t G L\left(d\left(\varphi_{o,k}\right)\right) |h_{o,k}|^2}{I_k} \geq \gamma_I \right\} \\ &= 1 - \underbrace{\Pr\left\{ |h_{o,k}|^2 < \frac{I_k \gamma_I}{P_t G L\left(d\left(\varphi_{o,k}\right)\right)} \right\}}_{P_o}. \end{aligned} \tag{18}$$

Note that P_o cannot be directly computed due to the randomness of both channel fading and aggregated interference. To address this issue, we first introduce Alzer's lemma in the following proposition.

Proposition 1. *Let g be a Gamma random variable with the shape parameter α and the scale parameter β. Then, its CDF can be tightly bounded as [24]*

$$\begin{cases} F_g(x) \leq \left[1 - \exp\left(-\mu x\right)\right]^{\alpha}, & \text{if } \alpha \leq 1 \\ F_g(x) > \left[1 - \exp\left(-\mu x\right)\right]^{\alpha}, & \text{if } \alpha > 1, \end{cases} \tag{19}$$

where $\mu = (\alpha!)^{-\frac{1}{\alpha}} / \beta$ and the equality holds when $\alpha = 1$.

As such, P_o in (18) can be computed as

$$\begin{aligned} P_o &= \Pr\left\{ |h_{o,k}|^2 < \frac{I_k \gamma_I}{P_t G L\left(d\left(\varphi_{o,k}\right)\right)} \right\} \\ &\overset{(a)}{\approx} \mathbb{E}_{I_k}\left[\left[1 - \exp\left(-\frac{\mu I_k \gamma_I}{P_t G L\left(d\left(\varphi_{o,k}\right)\right)} \right) \right]^{\alpha} \right] \\ &\overset{(b)}{=} \mathbb{E}_{I_k}\left[\sum_{z=0}^{\infty} \binom{\alpha}{z} (-1)^z \exp\left(-\frac{z \mu I_k \gamma_I}{P_t G L\left(d\left(\varphi_{o,k}\right)\right)} \right) \right] \\ &\overset{(c)}{=} \sum_{z=0}^{\infty} \binom{\alpha}{z} (-1)^z \mathcal{L}_{I_k}(s), \end{aligned} \tag{20}$$

where $s \triangleq \frac{z \mu \gamma_I}{P_t G L(d(\varphi_{o,k}))}$, step (a) follows from the approximated CDF of Gamma random variable according to Alzer's

lemma, step (b) follows from the generalized binomial theorem and step (c) follows from the LT of I_k. The convergence of this infinite series will be shown in Section IV-C.

Based on this, the analytical expression of P_{SIR} is derived as follows.

Proposition 2. *The capture probability in the presence of interference is approximately expressed as*

$$P_{SIR} \approx 1-\sum_{z=0}^{\infty}\binom{\alpha}{z}(-1)^z \exp\Bigg(2\pi R^2 p_k\lambda_k \times \Bigg(t_1\left[\frac{\left(\frac{t_1}{\epsilon}\right)^{\alpha}{}_2F_1\left(\alpha,\alpha+1;\alpha+2;-\frac{t_1}{\epsilon}\right)}{\alpha+1}-1\right]- t_2\left[\frac{\left(\frac{t_2}{\epsilon}\right)^{\alpha}{}_2F_1\left(\alpha,\alpha+1;\alpha+2;-\frac{t_2}{\epsilon}\right)}{\alpha+1}-1\right]\Bigg)\Bigg), \tag{21}$$

where $\epsilon \triangleq -\frac{s\beta\kappa P_t G c_0^2}{2R(R+H)}$, $t_1 \triangleq 1-\frac{(R+H)^2+R^2}{2R(R+H)}$, $t_2 \triangleq \cos\varphi_m - \frac{(R+H)^2+R^2}{2R(R+H)}$, *and* ${}_2F_1(\cdot,\cdot;\cdot;\cdot)$ *is the Gaussian hypergeometric function [25].*

Proof: See Appendix A. ∎

Remark 2: Different from the connection probability, the capture probability is closely related to the ED's density and active probability. The practical access probability could rapidly decrease with the increase of the ED's density and the active probability due to the escalated interference level.

C. Access Probability

By substituting (15) and (21) into (14), the analytical access probability can be obtained as

$$P_s \approx \left[1-\frac{1}{\Gamma(\alpha)}\gamma\left(\alpha,\frac{\sigma^2\gamma_k}{\beta P_t G L\left(d\left(\varphi_{o,k}\right)\right)}\right)\right] \times\left[1-\sum_{z=0}^{\infty}\binom{\alpha}{z}(-1)^z \exp\Bigg(2\pi R^2 p_k\lambda_k \times \Bigg(t_1\left[\frac{\left(\frac{t_1}{\epsilon}\right)^{\alpha}{}_2F_1\left(\alpha,\alpha+1;\alpha+2;-\frac{t_1}{\epsilon}\right)}{\alpha+1}-1\right]- t_2\left[\frac{\left(\frac{t_2}{\epsilon}\right)^{\alpha}{}_2F_1\left(\alpha,\alpha+1;\alpha+2;-\frac{t_2}{\epsilon}\right)}{\alpha+1}-1\right]\Bigg)\Bigg)\right]. \tag{22}$$

Note that (22) is computationally intensive and thereby we attempt to further simplify the analytical expression through approximating the impact of accumulative interference by that of the average interference. Specifically, since massive access is expected to occur in LoRa-based LEO satellite IoT networks due to the large satellite footprint, the aggregated interference for any class of EDs could likely converge to its mean value, i.e., $I_k \approx \bar{I}_k$. As a result, the approximate capture probability P_{SIR}° for LoRa EDs of class k can be given as

$$P_{SIR}^{\circ} = \Pr\left\{\frac{P_t G L\left(d\left(\varphi_{o,k}\right)\right)|h_{o,k}|^2}{\bar{I}_k} \geq \gamma_I\right\}. \tag{23}$$

Based on this, the analytical expression of P_{SIR}° is derived as follows.

Proposition 3. *The approximate capture probability under the impact of average co-SF interference is*

$$P_{SIR}^{\circ} \approx 1-\frac{1}{\Gamma(\alpha)}\gamma\left(\alpha,\frac{c_0^2\pi R\kappa p_k\lambda_k\alpha\gamma_I\ln\left(\frac{v_2}{v_1}\right)}{(R+H)L\left(d\left(\varphi_{o,k}\right)\right)}\right), \tag{24}$$

where $c_0 \triangleq \frac{c}{4\pi f_c}$, $v_1 \triangleq H^2$, *and* $v_2 \triangleq (R+H)^2+R^2-2R(R+H)\cos\varphi_m$.

Proof: See Appendix B. ∎

By substituting (15) and (24) into (14), the approximate access probability can be formulated as

$$P_s^{\circ} \approx \left[1-\frac{1}{\Gamma(\alpha)}\gamma\left(\alpha,\frac{\sigma^2\gamma_k}{\beta P_t G L\left(d\left(\varphi_{o,k}\right)\right)}\right)\right] \times\left[1-\frac{1}{\Gamma(\alpha)}\gamma\left(\alpha,\frac{c_0^2\pi R\kappa p_k\lambda_k\alpha\gamma_I\ln\left(\frac{v_2}{v_1}\right)}{(R+H)L\left(d\left(\varphi_{o,k}\right)\right)}\right)\right]. \tag{25}$$

IV. Numerical Results and Discussion

In this section, we validate our theoretical performance analysis through extensive Monte-Carlo simulations using MATLAB platform, which provides valuable insights into the uplink performance of LoRa-based LEO satellite IoT under practical system parameters. Furthermore, some open issues and future research directions are discussed, which can further shed light into the performance improvements of such a specific paradigm. Unless otherwise specified, the system parameter values used in our simulations are summarized in Table III, where the majority of these parameters are in accordance with [7], [10], [15], [18], [22], [23]. Moreover, the SF allocation scheme used in the simulations is fixed as random allocation scheme unless explicitly stated otherwise.

A. Interference-free Scenario

First of all, we will show the accuracy of approximating the SR channel gain by a corresponding Gamma random variable. Specifically, for two groups of parameters of SR fading, i.e., $m = 5.21$, $b_0 = 0.251$, $\Omega = 0.278$ and $m = 0.793$, $b_0 = 0.063$, $\Omega = 8.97\times10^{-4}$, the exact PDF of the SR channel gain given by (10) and the approximate PDF of the corresponding Gamma distribution given by (12) are plotted in Fig. 2. It can be seen that the approximation is very tight, which guarantees the effectiveness of our subsequent performance analysis.

Then, we investigate the access probability in the case of interference-free scenarios, which provides an upper bound for the practical uplink access performance. Herein, Fig. 3 and Fig. 4 present the uplink access probability of three different classes of LoRa EDs versus the EIRP, P_t, and orbit altitude, H, without the impact of interference, respectively. It can be observed that the simulation results are well matched with the theoretical results given by (15). Moreover, it can also be observed that the ideal access probability is monotonically increasing with P_t while monotonically decreasing with H, which is consistent with our intuition since the connection probability P_{SNR} is directly related to the link budget. Furthermore, it is apparent that in an interference-free scenario,

TABLE III
SIMULATION PARAMETERS

Notation	Values
R	6371 km
H	500 km
ψ	50°
λ	6×10^{-6}
k	$7, 8, 9, 10, 11, 12$
P_L	50 bytes
T_p	3600 s
m	5.21
b_0	0.251
Ω	0.278
f_c	868 MHz
B_W	125 kHz
P_t	16 dBm
N_F	6 dB
G	22.6 dBi
κ	10^{-3}
$\varphi_{o,k}$	0°
γ_k	$-6, -9, -12, -15, -17.5, -20$ dB
γ_I	6 dB

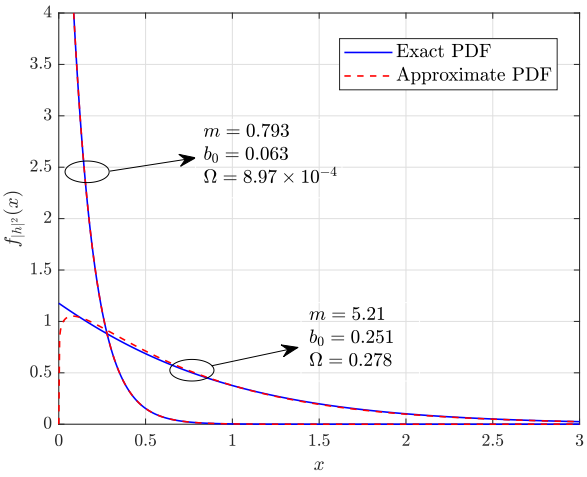

Fig. 2. Exact PDF of the SR channel gain and approximate PDF of the corresponding Gamma distribution.

the LoRa EDs with larger SF have better access performance since larger SF leads to a lower SNR demodulation threshold as shown in Table III. Hence, in an interference-free scenario, increasing the SF will lead to a better scalability performance due to the higher reception sensitivity.

B. Interference-limited Scenario

Fig. 5(a) and Fig. 5(b) demonstrate the access probability of different classes of LoRa EDs versus the ED's density for $H = 500$ km and $H = 1000$ km, respectively. Likewise, Fig. 6(a) and Fig. 6(b) demonstrate the access probability of different classes of LoRa EDs versus the satellite effective beamwidth for $H = 500$ km and $H = 1000$ km, respectively. It can be observed that the numerical results of the access

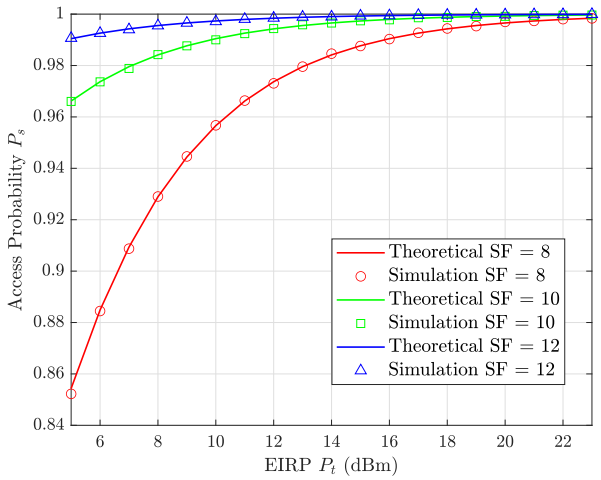

Fig. 3. Access probability of three classes of LoRa EDs versus the EIRP, P_t, without the impact of interference.

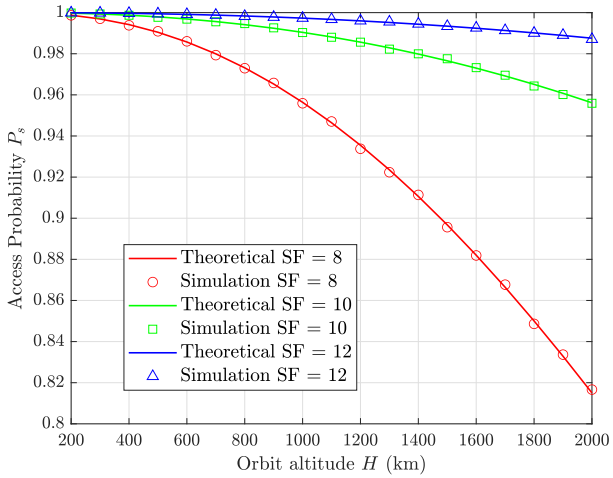

Fig. 4. Access probability of three classes of LoRa EDs versus the orbit altitude, H, without the impact of interference.

probability match well with the analytical results, which substantiates our proposed analytical framework once again. Moreover, the theoretical access probability based on the accumulative interference, i.e., P_s given by (22), is very close to the approximate access probability based on the average interference, i.e., P_s° given by (25), which shows that the aggregated interference I_k can be tightly approximated by its mean value $\bar{I}_k$.

Furthermore, as illustrated in Fig. 5 and Fig. 6, the access probability is a monotonically decreasing function of both λ and ψ, as the interference levels increase with λ and ψ. In particular, the access probability degrades exponentially with the increase of λ, showing that varying the ED's density has a significant impact on the uplink scalability performance of LoRa-based LEO satellite IoT systems. In addition, contrary to the interference-free scenario, the LoRa EDs with larger SF experience more severe performance degradation especially for larger value of the ED's density since higher SFs could be more prone to packet collisions due to the longer ToA

This article has been accepted for publication in IEEE Internet of Things Journal. This is the author's version which has not been fully edited and content may change prior to final publication. Citation information: DOI 10.1109/JIOT.2025.3571928

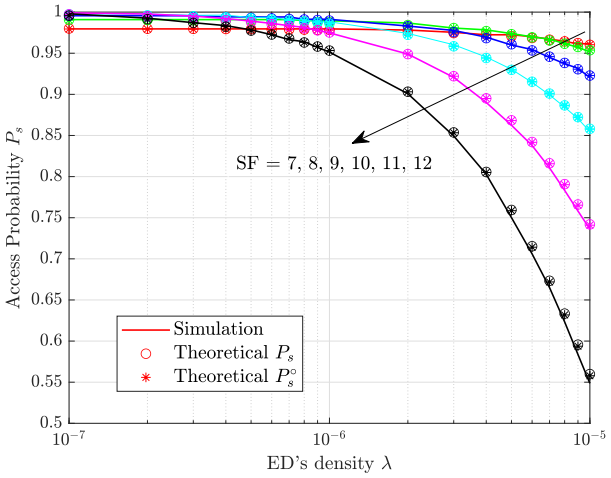

(a) $H = 500$ km

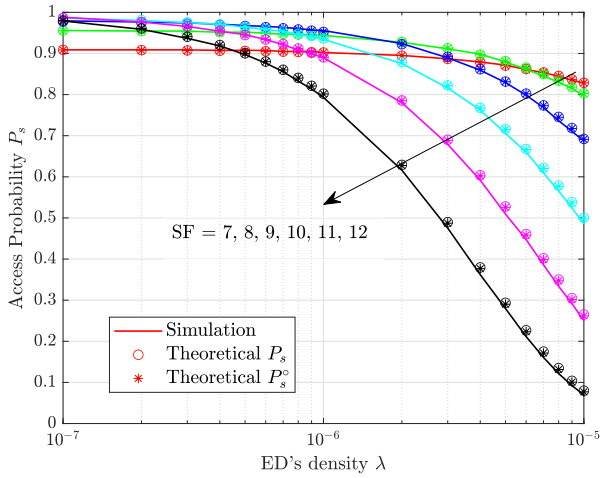

(b) $H = 1000$ km

Fig. 5. Access probability of different classes of LoRa EDs versus the ED's density with (a) $H = 500$ km and (b) $H = 1000$ km.

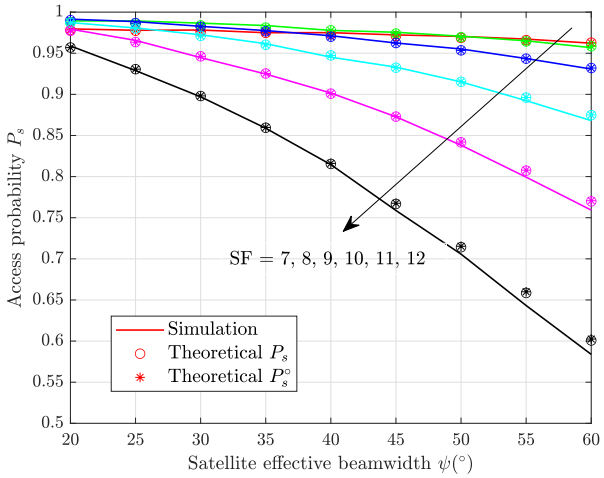

(a) $H = 500$ km

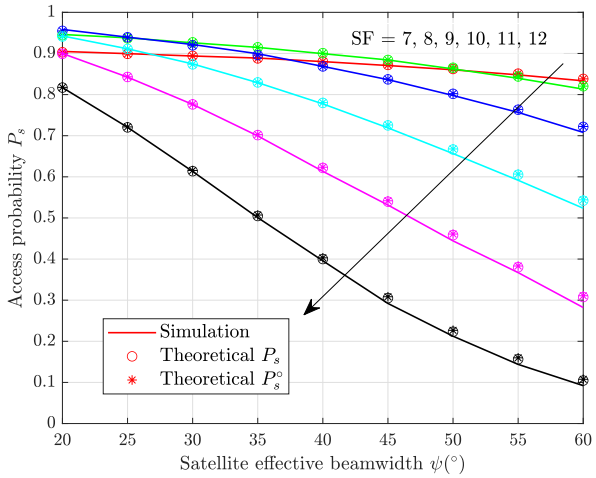

(b) $H = 1000$ km

Fig. 6. Access probability of different classes of LoRa EDs versus the satellite effective beamwidth with (a) $H = 500$ km and (b) $H = 1000$ km.

given by (6). Nonetheless, it should be noted that for small values of ED's density, like $\lambda = 10^{-7}$, the uplink scalability performance of LoRa EDs with smaller SFs could be better than that of LoRa EDs with larger SFs since, in this case, P_{SNR} will play a dominant role in determining the access probability, while the system performance will resemble that of the interference-free scenario.

Additionally, it can be observed that the uplink scalability performance degrades more rapidly for $H = 1000$ km compared to $H = 500$ km, due to the escalated large-scale fading. In particular, as shown in Fig. 6, the orbit altitude has a pronounced impact on the uplink scalability performance, especially for large satellite effective beamwidth, since for higher orbit altitude, the satellite footprint area increases more rapidly with ψ, thus leading to more severe interference and performance deterioration. This, in turn, indicates that we can control the interference level and improve the uplink scalability performance of LoRa-based LEO satellite IoT systems by adjusting the satellite orbit altitude and effective beamwidth. Moreover, the overall network performance can be further enhanced through the dense deployment of LEO satellites [23], which is an interesting topic left for future research.

Fig. 7 demonstrates the numerical access probability of three classes of LoRa EDs versus the ED's density for both random and fair-collision SF allocation schemes. It can be observed that compared to random SF allocation, fair-collision SF allocation can provide higher uplink access probability, i.e., better scalability performance, especially for larger SFs since it can guarantee a fair collision probability among all classes of EDs [15]. For example, the access probability is about 0.7 for $SF = 12$ under the fair-collision allocation scheme, while it drops below 0.1 under the random allocation scheme. This indicates that by designing and employing an appropriate SF allocation scheme, more efficient uplink access opportunities and better scalability performance of LoRa-based LEO satellite IoT systems can be reached.

This article has been accepted for publication in IEEE Internet of Things Journal. This is the author's version which has not been fully edited and content may change prior to final publication. Citation information: DOI 10.1109/JIOT.2025.3571928

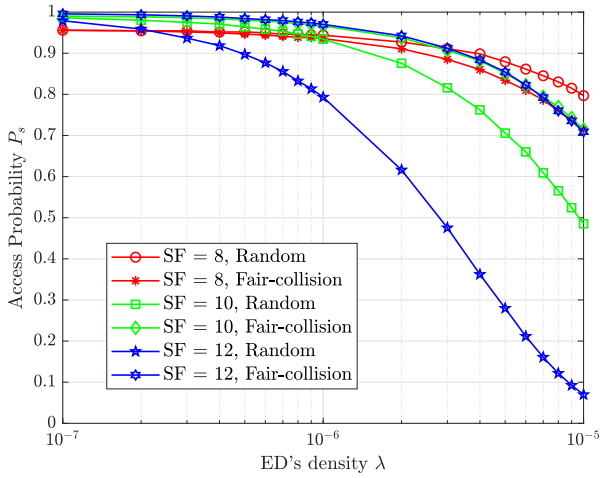

Fig. 7. Access probability of three classes of LoRa EDs versus the ED's density for both random and fair-collision SF allocation schemes.

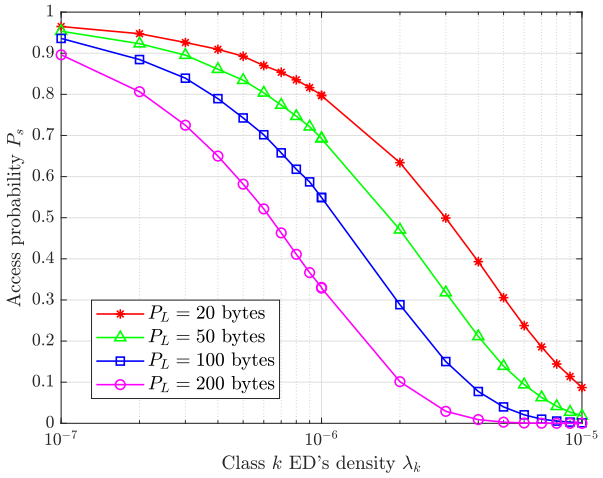

Fig. 9. Access probability versus the class k ED's density λ_k for different PHY payload length, P_L, with $SF = 12$.

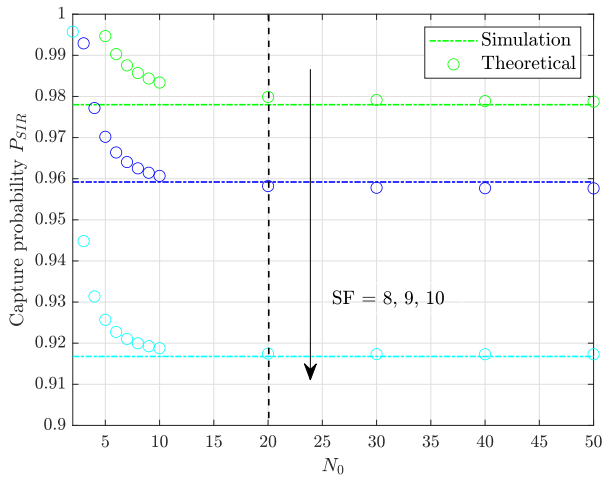

Fig. 8. Theoretical capture probability versus the first N_0 terms used in the calculation of the infinite series.

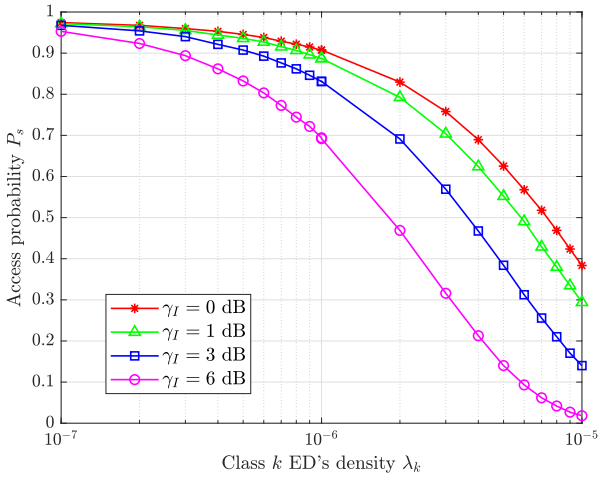

Fig. 10. Access probability versus the class k ED's density λ_k for different capture effect threshold, γ_I, with $SF = 12$.

C. Convergence Analysis and Justification

In this subsection, we provide the explanation behind the reason in the convergence of the infinite series in (20) and (21). According to Jensen's inequality [25], we have

$$\begin{aligned}&\mathbb{E}_{I_k}\left[-\exp\left(-\frac{\mu I_k \gamma_I}{P_t G L\left(d\left(\varphi_{o,k}\right)\right)}\right)\right]\\ &\leq \underbrace{-\exp\left(-\frac{\mu \bar{I}_k \gamma_I}{P_t G L\left(d\left(\varphi_{o,k}\right)\right)}\right)}_{\mathcal{I}},\end{aligned} \tag{26}$$

with

$$\begin{aligned}|\mathcal{I}| &\overset{(a)}{\approx} \exp\left(-\frac{\mu\pi R\kappa p_k \lambda_k \alpha\beta \ln\left(\frac{v_2}{v_1}\right)\gamma_I \left[d\left(\varphi_{o,k}\right)\right]^2}{R+H}\right)\\ &\overset{(b)}{\leq} \exp\left(-\frac{\mu\pi R\kappa p_k \lambda_k \alpha\beta \ln\left(\frac{v_2}{v_1}\right)\gamma_I H^2}{R+H}\right) < 1,\end{aligned} \tag{27}$$

where step (a) follows from the derivation of $\bar{I}_k$ as shown in Appendix B, while step (b) follows from the fact that $\varphi_{o,k} \in [0, \varphi_m]$ as stated in Section II-A. This guarantees the convergence of the infinite series in (20) according to the convergence property of binomial series [25], and thus validates the effectiveness of our derived analytical expressions for the capture probability. Herein, Fig. 8 shows the theoretical capture probability P_{SIR} versus the first N_0 terms used in the calculation of the infinite series. It can be observed that the theoretical capture probability P_{SIR} converges to fixed values for all considered SFs with $N_0 \geq 20$, which not only agrees well with the simulation results but also indicates rapid convergence. As such, the calculation of the theoretical capture probability P_{SIR} could be greatly simplified by using a small number of terms, but still with high accuracy.

D. Future Research Directions

In this subsection, we clarify some open issues and future research directions which can help us to dive deeper into the

This article has been accepted for publication in IEEE Internet of Things Journal. This is the author's version which has not been fully edited and content may change prior to final publication. Citation information: DOI 10.1109/JIOT.2025.3571928

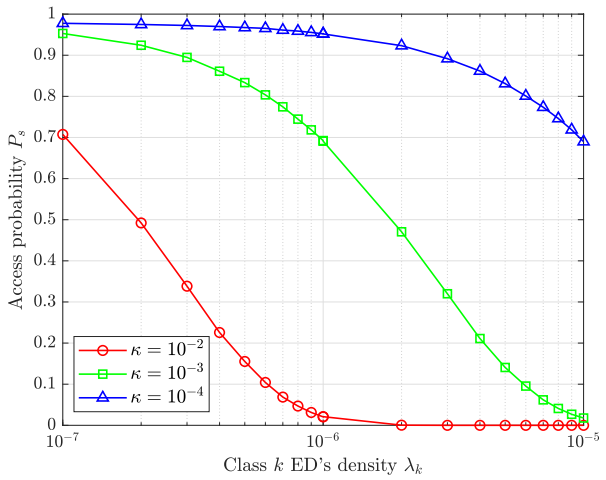

Fig. 11. Access probability versus the class k ED's density λ_k for different interference mitigation factor, κ, with $SF = 12$.

performance improvements of such a new paradigm.

1) PHY Layer: From the PHY layer perspective, the uplink scalability performance of LoRa-based LEO satellite IoT system can be effectively improved by suitable transceiver design.

On one hand, as depicted in Fig. 9, for a specific class of LoRa EDs, the access probability degrades with the increase of P_L as a longer PHY payload length will result in a longer ToA due to the low spectral efficiency of CSS modulation, and thus leading to higher probability of packet collisions and increased interference level. This phenomenon is more serious for larger SFs. Therefore, the uplink scalability performance of LoRa-based LEO satellite IoT system can be improved by adopting alternative CSS-based LoRa-like modulation schemes with higher spectral efficiency and enhanced data rate [26], [27].

On the other hand, as depicted in Fig. 10, the access probability improves with the decrease of γ_I, which is consistent with our intuition that a lower SIR demodulation threshold typically means a better collision resolution capability. As such, the uplink scalability performance of LoRa-based LEO satellite IoT system can be effectively improved by developing more efficient detectors in the presence of interference [28], [29]. Furthermore, the uplink scalability performance of LoRa-based LEO satellite IoT system can be further enhanced by employing advanced multi-user receivers instead of the current single-user receiver [30], [31].

2) MAC Layer: From the MAC layer perspective, the uplink scalability performance of LoRa-based LEO satellite IoT system can be significantly improved by appropriate protocol design. As a matter of fact, controlling the massive random access in a reasonable way is of great importance in the context of satellite IoT communications. The remarkable impact of interference mitigation factor on the uplink access probability of LoRa-based LEO satellite IoT system is shown in Fig. 11, which showcases that the uplink scalability performance can be significantly improved through link coordination. Hence, more network capacity can be unlocked by designing MAC layer protocols that are well-suited for LEO satellite IoT systems [32], [33]. Moreover, integrated approaches, i.e., combining PHY layer transceiver design and MAC layer protocol design in an efficient manner, also provide great potential for further improving the uplink scalability performance of LoRa-based LEO satellite IoT system [34].

V. Conclusion

In this paper, a novel analytical framework for characterizing the uplink access probability LoRa-based LEO satellite IoT was formulated based on spherical SG. In particular, both the channel characteristics of satellite link and the unique features of LoRa network were incorporated into the proposed system model, which gives an accurate performance evaluation of such a new paradigm. Closed-form analytical expressions for the uplink access probability of LoRa-based LEO satellite IoT system were derived. Extensive numerical simulations were conducted to verify the accuracy of our proposed analytical framework and also provide insightful guidelines for the practical design and implementation of LoRa-based LEO satellite IoT. Overall, we believe that our work will set the foundation for further exploration of LoRa technology in non-terrestrial networks.

Acknowledgment

This research work has been supported in part by the Australian Research Council Discovery Early Career Researcher Award (DECRA) - DE230101391.

Appendix A
Proof of Proposition 2

To derive the analytical expression of P_{SIR}, we first need to calculate the LT of I_k, which is presented as follows:

$$\begin{aligned}\mathcal{L}_{I_k}(s) &= \mathbb{E}_{I_k}\left[\exp\left(-s\sum_{i\in\Phi_k^A\setminus o}\kappa P_t G L\left(d\left(\varphi_{i,k}\right)\right)|h_{i,k}|^2\right)\right] \\ &= \mathbb{E}_{I_k}\left[\prod_{i\in\Phi_k^A\setminus o}\exp\left(-s\kappa P_t G L\left(d\left(\varphi_{i,k}\right)\right)|h_{i,k}|^2\right)\right] \\ &\overset{(a)}{=} \mathbb{E}_{\Phi_k^A\setminus o}\left[\prod_{i\in\Phi_k^A\setminus o}\left[1+s\beta\kappa P_t G L\left(d\left(\varphi_{i,k}\right)\right)\right]^{-\alpha}\right],\end{aligned} \tag{28}$$

where step (a) follows from the independence of i.i.d. channel fading and random point process and leverages the moment generating function (MGF) of a Gamma random variable.

According to the probability generating functional (PGFL) of PPP [35], we have

$$\mathbb{E}\left[\prod_{x\in\Phi} f(x)\right] = \exp\left(-\int_{\mathbb{R}^d}\left[1-f(x)\right]\Lambda(\mathrm{d}x)\right), \tag{29}$$

where Φ is a point process on $\mathbb{R}^d$, while $\Lambda(\cdot)$ is the intensity measure of Φ. As a result, $\mathcal{L}_{I_k}(s)$ can be further formulated as

$$\begin{aligned}\mathcal{L}_{I_k}(s) =& \mathbb{E}\left[\prod_{i\in\Phi_k^A\setminus o}\left[1+s\beta\kappa P_t G L\left(d\left(\varphi_{i,k}\right)\right)\right]^{-\alpha}\right]\\ =& \exp\Big\{2\pi R^2 p_k\lambda_k\times\\ &\underbrace{\int_0^{\varphi_m}\left(\left[1+s\beta\kappa P_t G L\left(d\left(\varphi\right)\right)\right]^{-\alpha}-1\right)\sin\varphi\mathrm{d}\varphi}_{\mathcal{I}_I}\Big\},\end{aligned} \tag{30}$$

where the integral $\mathcal{I}_I$ can be derived as

$$\begin{aligned}\mathcal{I}_I =& \int_0^{\varphi_m}\left(\left[1+s\beta\kappa P_t G L\left(d\left(\varphi\right)\right)\right]^{-\alpha}-1\right)\sin\varphi\mathrm{d}\varphi\\ =& \int_0^{\varphi_m}\frac{\sin\varphi}{\left(1+\frac{\epsilon}{\delta+\cos\varphi}\right)^{\alpha}}\mathrm{d}\varphi+\cos\varphi_m-1\\ \overset{(a)}{=}& \int_{\delta+\cos\varphi_m}^{\delta+1}\frac{1}{\left(1+\frac{\epsilon}{u}\right)^{\alpha}}\mathrm{d}u+\cos\varphi_m-1\\ \overset{(b)}{=}& t_1\left[\frac{\left(\frac{t_1}{\epsilon}\right)^{\alpha}{}_2F_1\left(\alpha,\alpha+1;\alpha+2;-\frac{t_1}{\epsilon}\right)}{\alpha+1}-1\right]-\\ & t_2\left[\frac{\left(\frac{t_2}{\epsilon}\right)^{\alpha}{}_2F_1\left(\alpha,\alpha+1;\alpha+2;-\frac{t_2}{\epsilon}\right)}{\alpha+1}-1\right],\end{aligned} \tag{31}$$

where step (a) follows from $\delta=-\frac{(R+H)^2+R^2}{2R(R+H)}$ and $u=\delta+\cos\varphi$, while step (b) follows from $t_1=1-\frac{(R+H)^2+R^2}{2R(R+H)}$ and $t_2=\cos\varphi_m-\frac{(R+H)^2+R^2}{2R(R+H)}$.

Therefore, the capture probability can be formulated according to (18) and (20) as

$$\begin{aligned}P_{SIR}\approx& 1-\sum_{z=0}^{\infty}\binom{\alpha}{z}(-1)^z\mathcal{L}_{I_k}(s)\\ =& 1-\sum_{z=0}^{\infty}\binom{\alpha}{z}(-1)^z\exp\Bigg(2\pi R^2 p_k\lambda_k\times\\ &\Bigg(t_1\left[\frac{\left(\frac{t_1}{\epsilon}\right)^{\alpha}{}_2F_1\left(\alpha,\alpha+1;\alpha+2;-\frac{t_1}{\epsilon}\right)}{\alpha+1}-1\right]-\\ & t_2\left[\frac{\left(\frac{t_2}{\epsilon}\right)^{\alpha}{}_2F_1\left(\alpha,\alpha+1;\alpha+2;-\frac{t_2}{\epsilon}\right)}{\alpha+1}-1\right]\Bigg)\Bigg).\end{aligned} \tag{32}$$

Appendix B
Proof of Proposition 3

According to the Campbell's theorem for sums [35], we have

$$\mathbb{E}\left[\sum_{x\in\Phi}f(x)\right]=\int_{\mathbb{R}^d}f(x)\Lambda(\mathrm{d}x), \tag{33}$$

where Φ is a point process on $\mathbb{R}^d$ and $\Lambda(\cdot)$ is the intensity measure of Φ. Therefore, the average co-SF interference $\bar{I}_k$ can be formulated as

$$\begin{aligned}\bar{I}_k =& \mathbb{E}_{I_k}\left[\kappa\sum_{i\in\Phi_k^A\setminus o}P_t G L\left(d\left(\varphi_{i,k}\right)\right)|h_{i,k}|^2\right]\\ \overset{(a)}{=}& 2\pi R^2\kappa p_k\lambda_k P_t G\int_0^{\varphi_m}L\left(d\left(\varphi\right)\right)\mathbb{E}_{|h|^2}\left[|h|^2\right]\sin\varphi\mathrm{d}\varphi\\ \overset{(b)}{\approx}& 2\pi R^2\kappa p_k\lambda_k P_t G\alpha\beta\underbrace{\int_0^{\varphi_m}L\left(d\left(\varphi\right)\right)\sin\varphi\mathrm{d}\varphi}_{\mathcal{I}_{II}},\end{aligned} \tag{34}$$

where step (a) follows from the fact that the i.i.d. channel fading is independent from the spatial random point process while step (b) follows the mean value of the approximated Gamma distribution of channel fading.

Moreover, the integral $\mathcal{I}_{II}$ can be derived as

$$\begin{aligned}\mathcal{I}_{II} =& \int_0^{\varphi_m}L\left(d\left(\varphi\right)\right)\sin\varphi\mathrm{d}\varphi\\ =& \int_0^{\varphi_m}\frac{\left(\frac{c}{4\pi f_c}\right)^2\sin\varphi}{\left(R+H\right)^2+R^2-2R\left(R+H\right)\cos\varphi}\mathrm{d}\varphi\\ \overset{(a)}{=}& \int_{\cos\varphi_m}^{1}\frac{\left(\frac{c}{4\pi f_c}\right)^2}{\left(R+H\right)^2+R^2-2R\left(R+H\right)u}\mathrm{d}u\\ \overset{(b)}{=}& \int_{v_1}^{v_2}\frac{\left(\frac{c}{4\pi f_c}\right)^2}{2R\left(R+H\right)v}\mathrm{d}v\\ =& \frac{c_0^2}{2R\left(R+H\right)}\ln\left(\frac{v_2}{v_1}\right),\end{aligned} \tag{35}$$

where step (a) follows from $u=\cos\varphi$, while step (b) follows from $v=\left(R+H\right)^2+R^2-2R\left(R+H\right)u$.

Consequently, the approximate capture probability can be formulated as

$$\begin{aligned}P_{SIR}^{\circ} =& \Pr\left\{\frac{P_t G L\left(d\left(\varphi_{o,k}\right)\right)|h_{o,k}|^2}{\bar{I}_k}\geq\gamma_I\right\}\\ =& 1-F_{|h_{o,k}|^2}\left(\frac{\bar{I}_k\gamma_I}{P_t G L\left(d\left(\varphi_{o,k}\right)\right)}\right)\\ \overset{(a)}{\approx}& 1-\frac{1}{\Gamma(\alpha)}\gamma\left(\alpha,\frac{c_0^2\pi R\kappa p_k\lambda_k\alpha\gamma_I\ln\left(\frac{v_2}{v_1}\right)}{\left(R+H\right)L\left(d\left(\varphi_{o,k}\right)\right)}\right),\end{aligned} \tag{36}$$

where step (a) leverages the approximated Gamma distribution of channel fading described in (11).

References

[1] Q. Yu, D. Mishra, H. Wang, D. He, J. Yuan, and M. Matthaiou, "Closed-form access probability analysis of LoRa-based LEO satellite IoT," accepted for presentation at *IEEE ICC 2025*.

[2] U. Raza, P. Kulkarni, and M. Sooriyabandara, "Low power wide area networks: An overview," *IEEE Commun. Surveys Tuts.*, vol. 19, no. 2, pp. 855-873, 2nd Quart., 2017.

[3] R. Marini, K. Mikhaylov, G. Pasolini, and C. Buratti, "Low-power wide-area networks: Comparison of LoRaWAN and NB-IoT performance," *IEEE Internet Things J.*, vol. 9, no. 21, pp. 21051-21063, Nov. 2022.

[4] J. P. S. Sundaram, W. Du, and Z. Zhao, "A survey on LoRa networking: Research problems, current solutions, and open issues," *IEEE Commun. Surveys Tuts.*, vol. 22, no. 1, pp. 371-388, 1st Quart., 2020.

[5] M. Centenaro, C. E. Costa, F. Granelli, C. Sacchi, and L. Vangelista, "A survey on technologies, standards and open challenges in satellite IoT," *IEEE Commun. Surveys Tuts.*, vol. 23, no. 3, pp. 1693-1720, 3rd Quart., 2021.

[6] L. Fernandez, J. A. Ruiz-De-Azua, A. Calveras, and A. Camps, "Assessing LoRa for satellite-to-Earth communications considering the impact of ionospheric scintillation," *IEEE Access*, vol. 8, pp. 165570-165582, Sep. 2020.

[7] M. Asad Ullah, K. Mikhaylov, and H. Alves, "Massive machine-type communication and satellite integration for remote areas," *IEEE Wireless Commun.*, vol. 28, no. 4, pp. 74-80, Aug. 2021.

[8] A. M. Zadorozhny *et al.*, "First flight-testing of LoRa modulation in satellite radio communications in low-Earth orbit," *IEEE Access*, vol. 10, pp. 100006-100023, Sep. 2022.

[9] J. A. Fraire, O. Iova, and F. Valois, "Space-terrestrial integrated Internet of things: Challenges and opportunities," *IEEE Commun. Mag.*, vol. 60, no. 12, pp. 64-70, Dec. 2022.

[10] O. Georgiou and U. Raza, "Low power wide area network analysis: Can LoRa scale?," *IEEE Wireless Commun. Lett.*, vol. 6, no. 2, pp. 162-165, Apr. 2017.

[11] A. Hoeller, R. D. Souza, O. L. Alcaraz López, H. Alves, M. de Noronha Neto, and G. Brante, "Analysis and performance optimization of LoRa networks with time and antenna diversity," *IEEE Access*, vol. 6, pp. 32820-32829, Jun. 2018.

[12] A. Mahmood, E. Sisinni, L. Guntupalli, R. Rondón, S. A. Hassan, and M. Gidlund, "Scalability analysis of a LoRa network under imperfect orthogonality," *IEEE Trans. Ind. Informat.*, vol. 15, no. 3, pp. 1425-1436, Mar. 2019.

[13] J. M. de Souza Sant'Ana, A. Hoeller, R. D. Souza, H. Alves, and S. Montejo-Sánchez, "LoRa performance analysis with superposed signal decoding," *IEEE Wireless Commun. Lett.*, vol. 9, no. 11, pp. 1865-1868, Nov. 2020.

[14] Z. Qin, Y. Liu, G. Y. Li, and J. A. McCann, "Performance analysis of clustered LoRa networks," *IEEE Trans. Veh. Technol.*, vol. 68, no. 8, pp. 7616-7629, Aug. 2019.

[15] L. -T. Tu, A. Bradai, Y. Pousset, and A. I. Aravanis, "On the spectral efficiency of LoRa networks: Performance analysis, trends and optimal points of operation," *IEEE Trans. Commun.*, vol. 70, no. 4, pp. 2788-2804, Apr. 2022.

[16] B. Al Homssi *et al.*, "Next generation mega satellite networks for access equality: Opportunities, challenges, and performance," *IEEE Commun. Mag.*, vol. 60, no. 4, pp. 18-24, Apr. 2022.

[17] R. Wang, M. A. Kishk, and M. -S. Alouini, "Ultra-dense LEO satellite-based communication systems: A novel modeling technique," *IEEE Commun. Mag.*, vol. 60, no. 4, pp. 25-31, Apr. 2022.

[18] C. C. Chan, B. Al Homssi, and A. Al-Hourani, "A stochastic geometry approach for analyzing uplink performance for IoT-over-satellite," in *Proc. IEEE ICC*, May 2022, pp. 1-6.

[19] A. K. Dwivedi, S. Chaudhari, N. Varshney, and P. K. Varshney, "Performance analysis of LEO satellite-based IoT networks in the presence of interference," *IEEE Internet Things J.*, vol. 11, no. 5, pp. 8783-8799, Mar. 2024.

[20] W. Zhou, T. Hong, X. Ding, and G. Zhang, "LoRa performance analysis for LEO satellite IoT networks," in *Proc. IEEE WCSP*, Oct. 2021, pp. 1-5.

[21] A. Talgat, M. A. Kishk, and M. -S. Alouini, "Stochastic geometry-based uplink performance analysis of IoT over LEO satellite communication," *IEEE Trans. Aerosp. Electron. Syst.*, vol. 60, no. 4, pp. 4198-4213, Aug. 2024.

[22] B. A. Homssi and A. Al-Hourani, "Modeling uplink coverage performance in hybrid satellite-terrestrial networks," *IEEE Commun. Lett.*, vol. 25, no. 10, pp. 3239-3243, Oct. 2021.

[23] H. Jia, C. Jiang, L. Kuang, and J. Lu, "An analytic approach for modeling uplink performance of mega constellations," *IEEE Trans. Veh. Technol.*, vol. 72, no. 2, pp. 2258-2268, Feb. 2023.

[24] H. Jia, Z. Ni, C. Jiang, L. Kuang, and J. Lu, "Uplink interference and performance analysis for megasatellite constellation," *IEEE Internet Things J.*, vol. 9, no. 6, pp. 4318-4329, Mar. 2022.

[25] A. Jeffrey and D. Zwillinger, *Table of Integrals, Series, and Products.* Amsterdam, The Netherlands: Elsevier, 2007.

[26] Q. Yu, D. He, Z. Lu, and H. Wang, "SSK-based PSK-LoRa modulation for IoT communications," *IEEE Open J. Commun. Soc.*, vol. 4, pp. 1487-1498, Jul. 2023.

[27] Q. Yu, D. He, Z. Lu, and H. Wang, "Layered group-based chirp spread spectrum modulation: Waveform design and performance analysis," *IEEE Trans. Commun.*, early access.

[28] K. Dakic, B. Al Homssi, S. Walia, and A. Al-Hourani, "Spiking neural networks for detecting satellite internet of things signals," *IEEE Trans. Aerosp. Electron. Syst.*, vol. 60, no. 1, pp. 1224-1238, Feb. 2024.

[29] A. A. Tesfay, S. Kharbech, E. P. Simon, and L. Clavier, "Signal denoising and detection for uplink in LoRa networks based on Bayesian-optimized deep neural networks," *IEEE Commun. Lett.*, vol. 27, no. 1, pp. 214-218, Jan. 2023.

[30] J. Tapparel, M. Xhonneux, D. Bol, J. Louveaux, and A. Burg, "Enhancing the reliability of dense LoRaWAN networks with multi-user receivers," *IEEE Open J. Commun. Soc.*, vol. 2, pp. 2725-2738, Dec. 2021.

[31] M. Xhonneux, J. Tapparel, A. Balatsoukas-Stimming, A. Burg, and O. Afisiadis, "A maximum-likelihood-based two-user receiver for LoRa chirp spread-spectrum modulation," *IEEE Internet Things J.*, vol. 9, no. 22, pp. 22993-23007, Nov. 2022.

[32] M. Afhamisis and M. R. Palattella, "SALSA: A scheduling algorithm for LoRa to LEO satellites," *IEEE Access*, vol. 10, pp. 11608-11615, Jan. 2022.

[33] S. Herrería-Alonso, M. Rodríguez-Pérez, R. F. Rodríguez-Rubio, and F. Pérez-Fontán, "Improving uplink scalability of LoRa-based direct-to-satellite IoT networks," *IEEE Internet Things J.*, vol. 11, no. 7, pp. 12526-12535, Apr. 2024.

[34] W. Xiao, M. Kaneko, N. El Rachkidy, and A. Guitton, "Integrating LoRa collision decoding and MAC protocols for enabling IoT massive connectivity," *IEEE Internet Things Mag.*, vol. 5, no. 3, pp. 166-173, Sept. 2022.

[35] M. Haenggi, *Stochastic Geometry for Wireless Networks*. Cambridge, U.K.: Cambridge Univ. Press, 2012.